ELSEVIER

Cesium migration in Hanford sediment: a multisite cation exchange model based on laboratory transport experiments

Carl I. Steefel*, Susan Carroll, Pihong Zhao, Sarah Roberts

Energy and Environment Sciences Directorate, Lawrence Livermore National Laboratory, 7000 East Avenue, Livermore, CA 94550, USA

Abstract

Cs$^+$ transport experiments carried out in columns packed with uncontaminated Hanford formation sediment from the SX tank farm provide strong support for the use of a multisite, multicomponent cation exchange model to describe Cs$^+$ migration in the Hanford vadose zone. The experimental results indicate a strong dependence of the effective Cs$^+$ K_d on the concentrations of other cations, including Na$^+$ that is present at high to extremely high concentrations in fluids leaking from the Hanford SX tanks. A strong dependence of the Cs$^+$ K_d on the aqueous Cs$^+$ concentration is also apparent, with retardation of Cs$^+$ increasing from a value of 41 at a Cs$^+$ concentration of 10^{-4} M in the feed solution to as much as 282 at a Cs$^+$ concentration of 5×10^{-7} M, all in a background of 1 M NaNO$_3$. The total cation exchange capacity (CEC) of the Hanford sediment was determined using ^{22}Na isotopic equilibrium exchange in a flow-through column experiment. The value for the CEC of 120 µeq/g determined with this method is compatible with a value of 121.9 µeq/g determined by multi-cation elution. While two distinct exchange sites were proposed by Zachara et al. [Geochim. Cosmochim. Acta 66 (2002) 193] based on binary batch exchange experiments, a third site is proposed in this study to improve the fit of the Cs$^+$–Na$^+$ and Cs$^+$–Ca$^+$ exchange data and to capture self-sharpened Cs$^+$ breakthrough curves at low concentrations of Cs$^+$. Two of the proposed exchange sites represent frayed edge sites (FES) on weathered micas and constitute 0.02% and 0.22% of the total CEC. Both of the FES show a very strong selectivity for Cs$^+$ over Na$^+$ ($K_{Na-Cs} = 10^{7.22}$ and $10^{4.93}$, respectively). The third site, accounting for over 99% of the total CEC, is associated with planar sites on expansible clays and shows a smaller Na$^+$–Cs$^+$ selectivity coefficient of $10^{1.99}$.

Parameters derived from a fit of binary batch experiments alone tend to under predict Cs$^+$ retardation in the column experiments. The transport experiments indicate 72–90% of the Cs$^+$ sorbed in experiments targeting exchange on FES was desorbed over a 10- and 24-day period,

---

* Corresponding author. Tel.: +1-925-424-9807; fax: +1-925-422-3925.
  E-mail address: steefel@llnl.gov (C.I. Steefel).

respectively. At high Cs^+ concentrations, where sorption is controlled primarily by exchange on planar sites, 95% of the Cs^+ desorption was desorbed. Most of the difficulty in desorbing Cs^+ from FES is a result of the extremely high selectivity of these sites for Cs^+, although truly irreversible sorption as high as 23% was suggested in one experiment. The conclusion that Cs^+ exchange is largely reversible in a thermodynamic sense is supported by the ability to match Cs^+ desorption curves almost quantitatively with an equilibrium reactive transport simulation. The model for Cs^+ retardation developed here qualitatively explains the behavior of Cs^+ in the Hanford vadose zone underneath a variety of leaking tanks with differing salt concentrations. The high selectivity of FES for Cs^+ implies that future desorption and migration is very unlikely to occur under natural recharge conditions.

1. Introduction

[137]Cs, formed as a by-product of processing of uranium fuels, is a major component of high level nuclear wastes in the United States and other countries around the world. In a few cases, large amounts of ^{137}Cs have been released into the environment accidentally, as at Chernobyl in the former Soviet Union due to a reactor accident and at the Hanford site in the USA as a result of leaking of high level waste (HLW) storage tanks. While the migration of Cs^+ is limited typically in subsurface materials by its strong retardation (Reynolds et al., 1982; Guttierrez and Fuentes, 1993; Thirlwell et al., 1995; AntonopoulosDomis et al., 1995, 1997; Giani and Helmers, 1997; Chibowski et al., 1999; Klyashtorin et al., 1999; Szerbin et al., 1999; Rafferty et al., 2000), recent observations of leaks from the SX tank farm at Hanford indicate that ^{137}Cs has migrated locally to significantly greater depths than expected (Serne et al., 2001a,b). Retardation of the Cs^+ plume relative to non-reactive contaminants like nitrate and technetium in the case of some tanks leaks is minor, with estimates of retardation ranging from about 2 to 3 (Ward et al., 1997).

Explanations for the apparent enhanced migration of Cs^+ have fallen into two broad categories: (1) those based on physical processes, such as fast flow pathways or bypassing of exchange sites in immobile zones under low liquid saturation conditions, and (2) those based on chemical processes related to the very high electrolyte contents, high pH, and high temperature of the leaking tank fluids at the SX tank farm. It is well established that Cs^+ is normally strongly sorbed by the clays and micas (Sawhney, 1970; Francis and Brinkley, 1976; Brouwer et al., 1983; Poinssot et al., 1999; Zachara et al., 2002). Cs^+ sorbs via ion exchange reactions as a hydrated cation on planar sites on expansible clays like smectite (Sawhney, 1970; Brouwer et al., 1983; Zachara et al., 2002). In addition, Cs^+ is sorbed very selectively to FES on weathered micas (Jackson, 1963; Rich and Black, 1964; Zachara et al., 2002). EXAFS spectra suggest that the Cs^+ sorbed on the mica edge sites do so as inner-sphere dehydrated surface complexes (Kemner et al., 1997). Cations with low hydration energies (e.g., K^+, Rb^+, and NH_4^+) will compete mostly strongly with Cs^+ for the FES, while cations with stable hydration shells (e.g., Ca^+, Mg^+, and Sr^+) will not. In terms

of the transport behavior of Cs^+, the implication of these studies is that the retardation of ^{137}Cs in the subsurface will be a strong function of the relative proportions and abundances of expansible clays and micas.

Some previous studies have suggested that the retardation of Cs^+ might be decreased by competition with other dissolved constituents, including Na^+ (Voudrias et al., 1993; Saiers and Hornberger, 1996), K^+, and NH_4 (Sobolev, 1996). Chromatographic separation of various species in vertical boreholes at the SX tank farm, including ^{137}Cs, and K^+, Na^+, Ca^{2+}, and NO_3^- (acting as a tracer), suggested that Cs^+ migration might be described with a multicomponent ion exchange model (Serne et al., 2001a,b; Zachara et al., 2002). The chromatographic pattern is most clearly displayed in the plume developed from a leak of the SX-115 tank (Serne et al., 2001a). Here, Cs^+ is retarded with respect to both K^+ and Na^+, which are in turn slightly retarded with respect to Ca^{2+}, Mg^{2+}, and NO_3^-. The chromatographic sequence of $Cs^+ > Na^+, K^+ > NO_3^-, Ca^{2+}, Mg^{2+}$ is qualitatively what is expected based on a cation exchange model given the commonly reported values for the selectivity coefficients for these cations (e.g., Appelo and Postma, 1993) and a salinity front that is dominated by $NaNO_3$ (the primary electrolyte in the Hanford tank leaks) moving through Ca^{2+}- and Mg^{2+}-bearing sediments.

Observations of the apparently enhanced mobility of Cs^+ at Hanford led Zachara et al. (2002) to conduct a systematic series of binary batch exchange experiments over a wide range of Cs^+, Na^+, K^+, and Ca^{2+} concentrations using composite Hanford sediment from the SX tank farm. Based on their experimental results, Zachara et al. (2002) suggested a two-site multicomponent ion exchange model could be used to predict Cs^+ sorption and retardation in Hanford sediments. Their experimental data suggested a site with a very high affinity for Cs^+ relative to the other cations that was present at low concentrations (about 0.03 μeq/g sediment or 0.03% of the total CEC) and a more abundant site (50–80 μeq/g) that had a relatively lower affinity for Cs^+. They correlated the first site with specific sorption on FES on micas, while the second was believed to represent non-specific (hydrated) sorption on surfaces of expansible clays.

In this paper, we report the results of Cs^+ transport experiments using flow-through columns packed with the same composite of Hanford Formation sediment from the SX tank farm that was used by Zachara et al. (2002) in their batch exchange experiments. One of the specific objectives of the study was to test the ability of a multicomponent cation exchange model derived from batch experiments to predict Cs^+ transport. To the extent that the batch experiments could not completely explain the mobility of Cs^+ in the column experiments, the Cs^+ transport experiments were used to derive a set of cation exchange parameters (site concentrations and selectivity coefficients) that could be used to predict migration of Cs^+ in the field at Hanford. The column experiments were also used to provide a direct test of the reversibility of exchange by following the Cs^+ injection with elution of the column with concentrated $NaNO_3$ or $NaOH$ electrolyte alone. The Cs^+ injection experiments included: (1) binary Cs^+–Na^+ exchange experiments at $NaNO_3$ concentrations of 1 and 5 M, and Cs^+ concentrations of 5×10^{-7}, 5×10^{-6}, and 10^{-4} M; (2) a ternary Cs^+–K^+–Na^+ exchange experiment in 0.1 M KNO_3, 0.9 M $NaNO_3$, and 10^{-4} M Cs^+; and (3) an experiment using 1 M $NaOH$ to determine Cs^+ mobility under high base conditions. Initial elution of the column with either $NaNO_3$ or KNO_3 was used to determine the cation exchange capacity (CEC) by measuring the quantity of Ca^{2+},

Mg^{2+}, Na^+, and K^+ displaced from the sediment. Separate batch and column ^{22}Na exchange experiments were also used to determine the CEC.

A key aspect of the present study is to develop a multicomponent cation exchange model that can be used to simulate Cs^+ transport in the vadose zone below the leaking Hanford tanks. In this respect, the present study follows a number of previous studies that have used multicomponent cation exchange models to describe reactive transport (Valocchi et al., 1981a,b; Appelo and Willemsen, 1987; Charbeneau, 1988; Appelo et al., 1990, 1993; Griffioen et al., 1992; Appelo and Postma, 1993; Appelo, 1994, 1996; Bond, 1997; Voegelin et al., 2000). To the extent that a multicomponent ion exchange model is successful, it can be used to describe Cs^+ mobility over a large range of salt concentrations where the Cs^+ distribution coefficient (K_d) is not expected to be constant.

2. Experimental procedures

A total of 71-cm diameter column experiments using uncontaminated Hanford sediments were carried out at 25 °C to investigate the mobility of Cs^+ (Table 1). A Hanford formation homogenized composite sample from S-SX RCRA wells (Zachara et al., 2002) was used as the experimental medium. The sediment was lightly crushed at Pacific Northwest National Laboratory to pass through a 2-mm sieve, air-dried and mixed thoroughly. For this study, no further fractionation of the sediments was conducted. Zachara et al. (2002) further treated the composite sediment with a Na-acetate rinse to remove carbonates, while the sediments used in this study did not undergo such a rinse.

The sediments were loaded into a reactor column (1×15 cm) filled with distilled and deionized water. Sediment density was determined to be 2.67 g cm^{-3} by volume displacement. The elution experiments consisted of three phases. In the pretreatment phase, the background electrolyte (either $NaNO_3$ or KNO_3) was passed through the column to displace K^+ or Na^+, Ca^{2+}, and Mg^{2+} on the sediment exchange sites. The bulk of the exchange was achieved in seven to ten pore volumes. The pretreatment phase of the experiment also provided an independent measure of the sediment CEC. The pretreatment phase was followed by a stage where CsI and $NaNO_3$ (or mixed KNO_3–$NaNO_3$, or NaOH) solution was passed through the sediment column to measure Cs^+ retardation from the

Table 1
Summary of Cs^+ column experiments on Hanford sediment

Inlet salt solution	Inlet Cs (M)	Flow rate (ml min^{-1})	Darcy flux (cm min^{-1})	Sediment-solution ratio (g/l)	Porosity (%)
5 M NaNO$_3$	10^{-4}	0.1	0.121	3921.8	40.5
1 M NaNO$_3$	10^{-4}	0.1	0.113	3529.0	38.2
1 M NaNO$_3$	10^{-4}	0.02	0.025	3682.9	40.4
0.1 M KNO$_3$ 0.9 M NaNO$_3$	10^{-4}	0.1	0.113	3483.5	43.4
1 M NaOH	10^{-4}	0.02	0.023	4195.1	38.9
1 M NaNO$_3$	5×10^{-6}	0.1	0.121	3438	43.7
1 M NaNO$_3$	5×10^{-7}	0.1	0.113	3818.1	41.1

breakthrough curve. The final phase was a Cs^+ desorption experiment in which the background electrolyte solution without CsI was passed through the sediment column to displace Cs^+ from the exchange sites. Iodide was used to obtain the dispersivity of the columns.

The cation exchange capacity of the Hanford sediments collected at the SX tank farm was measured in several ways. First, ^{22}Na isotopic equilibrium batch experiments following the approach of Turner et al. (1996) were carried out in triplicate. Sediments were rinsed repeatedly with 2 mM $NaNO_3$ until a constant conductivity was achieved to saturate exchange sites with Na^+. The dry, treated sediments were then reacted in 2 mM $NaNO_3$ spiked with ^{22}Na (10^5 dpm/ml $^{22}Na–NaNO_3$) for 24 h. After equilibration, the suspensions were centrifuged, and the supernatant was filtered and analyzed for ^{22}Na by liquid scintillation and total Na by inductively coupled argon plasma emission spectroscopy (ICP-AES). These experiments were intended to duplicate the conditions of isotopic exchange experiments carried out by Zachara et al. (2002) and they gave very similar results. The cation exchange capacity was also determined from the equivalent sum of Ca^{2+}, K^+, Mg^{2+}, and Na^+ eluted with 1 M $NaNO_3$ and KNO_3 flushes of the sediments in the pretreatment phase of the experiments. This approach is similar to that described by Griffioen et al. (1992), Appelo and Postma (1993), and Appelo (1996), and relies on integration of the cation elution curve. Finally, the CEC was determined by ^{22}Na isotopic equilibrium in a flow-through column using 1 M $NaNO_3$, because the first two techniques yielded contradictory results. In this experiment, several pore volumes of 1 M $NaNO_3$ solution were flushed through the column to saturate the sediment column with Na^+ prior to injecting a ^{22}Na spiked solution of 1 M $NaNO_3$. The mass of ^{22}Na on exchange sites was determined by integrating the ^{22}Na elution curve and subtracting this from the integrated iodide elution curve, which was shown independently to behave as a non-reactive tracer. With the assumption of isotopic equilibrium between the ^{22}Na and the bulk Na on exchange sites, the total CEC can be calculated by assuming that the accessible exchange sites are occupied by Na^+.

Cs^+ was analyzed by inductively coupled plasma mass spectrometry (ICP-MS), Ca^{2+} and Mg^{2+} by ICP-AES, Na^+ and K^+ by flame atomic adsorption spectroscopy (flame AA), I^- by ion selective electrode, and ^{22}Na by liquid scintillation counting. pH was measured with a glass combination electrode and, in the high pH experiment, by Gran plot titration. The pH of the injection solutions in the circumneutral pH experiments were generally about 7.0, while the effluent showed a pH about one unit higher (7.9–8.1). The experiment using 1 M NaOH showed a significant drop in pH during the pre-flush stage, and then essentially no change during the Cs^+ sorption and desorption stage.

3. Modeling procedures

Distribution of species calculations and the simulations of multicomponent ion exchange and transport in the column experiments were carried out with the general purpose reactive transport code CRUNCH (Steefel, in preparation), a combined and updated Fortran 90 version of the codes GIMRT and OS3D (Steefel and Yabusaki, 1996; Steefel, 2001). While the code includes a much broader set of capabilities, in this

application, it is used to couple multicomponent, multisite ion exchange, aqueous complexation, and advective and dispersive transport.

Two sets of selectivity coefficients and exchange site concentrations were used to carry out the reactive transport simulations. One set of parameters was determined from a global fit of the batch Cs^+–Na^+, Cs^+–K^+, and Cs^+–Ca^{2+} exchange experiments at background electrolyte concentrations of 5 M $NaNO_3$ or less carried out by Zachara et al. (2002). These are referred to as the "batch parameters". The other set of selectivity coefficients and site concentrations was determined from both batch and column experiments, with weighting of the column experiments by a factor of 100 in the optimization procedure. These are referred to as the "column-weighted parameters". The weighting was carried out so as to resolve the discrepancies between fits based on the batch and column experiments. The column experiments were not used by themselves because they did not cover the entire range of concentrations of interest. The fits were carried out in all cases using the logarithms of the concentrations to avoid weighting of samples with higher concentrations. The column experiments were included by using the arrival time of the mean Cs^+ concentration ($C/C_0 = 0.5$) to determine a retardation factor, R_f. Since the experiments were carried out with a constant injection rate and chemical composition of the feed solution, a linear distribution coefficient applies in this case. Noting that the retardation, R_f, as measured in the column experiments is defined by:

$$R_f = 1 + \frac{\rho_B K_d}{\phi} = 1 + K_d',$$ (1)

where ρ_B is the bulk dry density of the sediment (g cm^{-3}), ϕ is the porosity, K_d is the distribution coefficient in units of ml g^{-1}, and K_d' is the dimensionless distribution coefficient (mol/l Cs^+ sorbed divided by the mol/l Cs^+ in the aqueous phase), the measured retardation of Cs^+ can be used to calculate partitioning of Cs^+ between the aqueous phase and exchange sites (K_d'). The aqueous concentration of Cs^+ and other species are used as input to the optimization calculation, while the sorbed Cs^+ is used as a constraint in a similar fashion to its use in fitting batch exchange experiments.

The fitting was carried out with the nonlinear optimization program PEST (Doherty et al., 1994) used in conjunction with distribution of species calculations carried out by CRUNCH. The resulting parameter set is then fully compatible with the reactive transport simulations of Cs^+ migration in the column experiments. The primary difference between these fits to the batch data and those presented by Zachara et al. (2002) is that the fit presented here is global, using a single set of exchanger concentrations for the multicomponent quaternary system (Cs^+–Na^+–K^+–Ca^{2+}), despite the fact that the original batch data is binary. In addition, these fits include activity coefficient corrections (described below) and aqueous complexation. Aqueous complexation, for example, is significant at $Ca(NO_3)_2$ concentrations of 0.5 M.

Multicomponent cation exchange was formulated using the Gaines–Thomas activity convention, which assumes a reaction stoichiometry of the following form (Appelo and Postma, 1993):

$$Cs^+ + 1/m MX(i)_m \leftrightarrow CsX(i) + 1/m M^{m+},$$ (2)
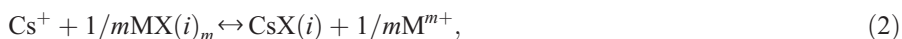
where M is the competing cation (Na^+, K^+, Ca^{2+}), m is its charge, and $X(i)$ refers to the ith type of exchange site. In the Gaines–Thomas convention, each exchange site, $X(i)$, has a charge of -1. The activities of adsorbed species correspond to the charge equivalent fractions, $\beta(i)_M$,

$$\beta(i)_M = \frac{z_M q(i)_M}{\sum\limits_M z_M q(i)_M} = [X(i)_M], \tag{3}$$

where z_M is the charge of cation M, $q(i)_M$ is the concentration of adsorbed cation M in exchange site i (mol/g), and the square brackets denote activities. The exchange reactions can then be used to write a mass action equation for binary Cs–M exchange:

$$K_{M/Cs} = \frac{\beta(i)_M^{1/m}[Cs^+]}{\beta(i)_{Cs}[M^{m+}]^{1/m}} = \frac{[X(i)_M]^{1/m}[Cs^+]}{[X(i)_{Cs}][M^{m+}]^{1/m}}. \tag{4}$$

In a single-site ion exchange model, the CEC is equal to the sum of the charge equivalent concentrations of the adsorbed cations:

$$CEC = \sum_M z_M q_M, \tag{5}$$

while in a multisite model, the CEC is the charge summed over all of the cation exchange sites (Cernik et al., 1996; Voegelin et al., 2000)

$$CEC = \sum_i \sum_M z_M q(i)_M, \tag{6}$$

As noted by Zachara et al. (2002), multiple exchange sites are needed to capture the large range in the distribution coefficient for Cs^+ as a function of Cs^+ concentration. Zachara et al. (2002) used a two-site model to fit the data, basing this in part on the physical evidence for the existence of at least two sites with very different affinities for Cs^+, one associated with the frayed edges sites (FES) on weathered micas and the other with the surfaces of expansible layer silicates. Spectrographic evidence for the existence of the Cs^+ sorption on micas has been presented by McKinley et al. (2001). In this work, fits based on a two-site and a three-site models were compared. In the fitting procedure, we assumed that the total CEC measured in the ^{22}Na column experiment represents the abundant, low affinity planar sites and fitted the exchange capacity for the less abundant, high affinity mica site (two-site model) or sites (three-site model). This is a reasonable approach to the extent that Site 1 in the case of the two-site model or Sites 1 and 2 in the three-site model comprise less than 1% of the total cation ion exchange capacity of the Hanford sediments at the SX tank farm.

A Debye–Huckel formulation was used to calculate activity coefficients. This approach was augmented with fitting parameters for ion pair formation to describe solution activities accurately in the highly concentrated and variable Cs^+–Na^+–K^+–Ca^{2+}–NO_3^- system found at the SX tank farm. Free cation activities were calculated by adjusting the log K_s

(equilibrium constants) for the ion pairs $CsNO_3(aq)$, $Ca(NO_3)_2(aq)$, and $NaNO_3(aq)$ to match ion activities (not activity coefficients) determined with the Pitzer approach as implemented in the code GMIN (Felmy, 1995). Ion pair formation, therefore, is described with effective equilibrium constants that incorporate the effects of ion interaction parameters in the Pitzer approach. The cation activities calculated by GMIN were used as "observations" to be matched by adjusting the effective equilibrium constants for the ion pair reactions in the global fitting procedure. While this method cannot be recommended as a general substitute for the full Pitzer approach, it captures the change in major cation activities over the concentration range of interest in the column experiments.

It was also necessary to include an empirical activity coefficient, γ, for the various Cs^+ exchange species in order to capture the ionic strength dependence of the exchange. This relatively small correction took the form of a constant, κ, multiplied by the ionic strength, I:

$$\ln\gamma_{Cs-X} = \kappa I \tag{7}$$

which affects only the Cs^+ exchange species.

Transport processes treated in the simulation of the experiments include advection and dispersion. Advection was simulated with an explicit third-order TVD (total variation diminishing) scheme (Datta-Gupta et al., 1991; Steefel and MacQuarrie, 1996). The simulations were run in every case at a Courant number of 1, in which case the TVD reverts to an explicit fully upwind approach. If the explicit upwind approach is run at a Courant number of 1, it is exact (Celia and Gray, 1992) and is equivalent to a mixing cell model. The accuracy of CRUNCH in modeling multicomponent ion exchange and transport was verified by comparing results with those produced by the code PHREEQC (Parkhurst, 1995) on ion exchange-transport examples included in the PHREEQC distribution. All of the simulations used 100 equally spaced grid cells to discretize the one-dimensional columns (typically 15 cm in length).

4. Results and discussion

4.1. Determination of the CEC for Hanford sediments at the SX tank farm

A CEC of 121.9 µeq/g was determined from the equivalent sum of the cations Ca^{2+}, Mg^{2+}, K^+, and Na^+ eluted by a pre-flush of the Hanford sediment using either 1 M $NaNO_3$ or 1 M KNO_3 (Fig. 1A and Table 2). Batch isotopic exchange experiments using ^{22}Na carried out in 2 mM $NaNO_3$ solutions, in contrast, yielded a substantially lower estimate of the CEC of 46 µeq/g of Hanford sediment, in close agreement with similar determinations presented by Zachara et al. (2002). It is not likely that the higher CEC for the cation elution experiments is an artifact of background concentration of cations or transient dissolution of carbonate, since a value of 120 µeq/g was determined based on ^{22}Na elution from the column (Fig. 1B). In addition, salts that might have contributed to a higher CEC determination were not observed in the original rinse with distilled water. The flow-through ^{22}Na exchange method also makes use of multiple pore volumes to fully exchange the sites. The extent of exchange can be verified directly from the elution curve (Fig. 1B). In contrast, the batch ^{22}Na exchange determination, which used a relatively low total concentration of 2 mM $NaNO_3$, may not
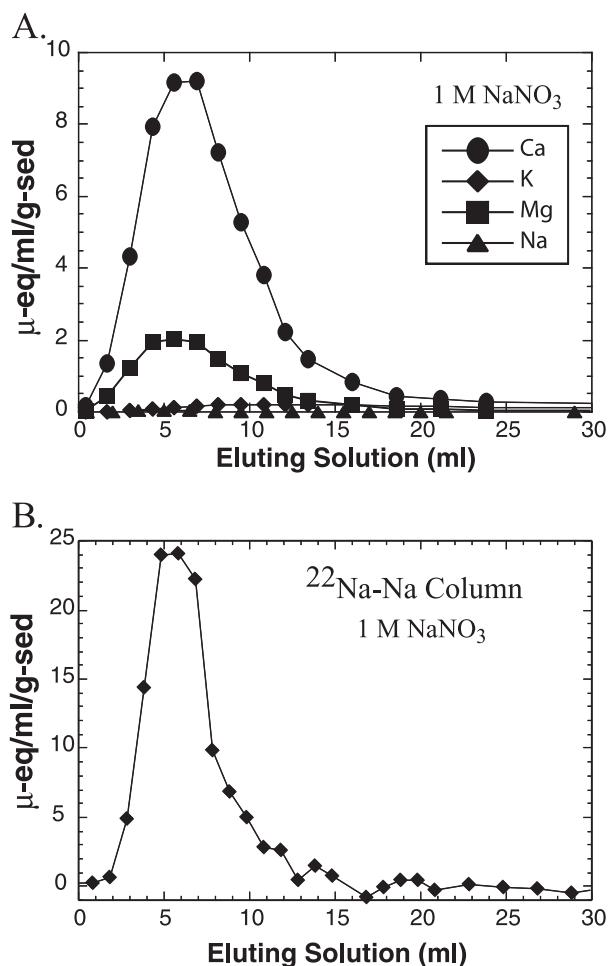
Fig. 1. (A) CEC of sediment from the SX tank farm at Hanford determined by cation elution and (B) [22]Na isotopic exchange determination of CEC.

have displaced all of the other cations on exchange sites, thus yielding an anomalously low CEC determination. For these reasons, and because of the compatibility with the determination based on cation elution, the [22]Na column result was considered the most reliable. Accordingly, a value of 120 μeq/g was used for the planar sites, with the assumption (to be confirmed) that the FES site(s) would constitute 1% or less of the total CEC.

4.2. Determination of column dispersivity

Iodide was used as a non-reactive tracer to determine the dispersivity of the column. The non-reactivity of iodide was verified by comparing iodide breakthrough in columns with and without sediment to a determination of the pore volume made gravimetrically. As

Table 2
Summary of cation elution results for Hanford sediment

Electrolyte	Na$^+$ (µeq/g)	K$^+$ (µeq/g)	Ca^{2+} (µeq/g)	Mg^{2+} (µeq/g)	Total (µeq/g)
1 M KNO$_3$	2.0		79.7	11.2	
1 M KNO$_3$	33.0		75.0	13.8	
1 M NaNO$_3$		5.6	89.3	16.7	
1 M NaNO$_3$		5.5	81.3	17.4	
5 M NaNO$_3$		10.3	85.0	17.5	
Average	17.5	7.0	82.1	15.3	121.9

a comparison, tracer experiments carried out with sediment-filled and empty columns showed iodide breakthroughs separated by 5.2 ml of fluid, while the pore volume determined gravimetrically was 5.1 ml.

Fig. 2 shows iodide breakthrough curves for experiments carried out at flow rates of 0.02 and 0.1 ml/min plotted as a function of pore volumes. While there is some scatter in the data, the elution curves are matched reasonably well using a dispersivity of 1 cm, although the experiment carried out with 5 M NaNO$_3$ (unfilled squares) shows a better match with a dispersivity of about 3 cm. A value for the dispersivity of 1 cm was used in all the simulations discussed below. Note that the iodide shows a slightly "non-ideal" breakthrough curve at concentrations above about $C/C_0 = 0.8$. The change in slope of the iodide breakthrough, first steep and then more gradual, is characteristic of the behavior of
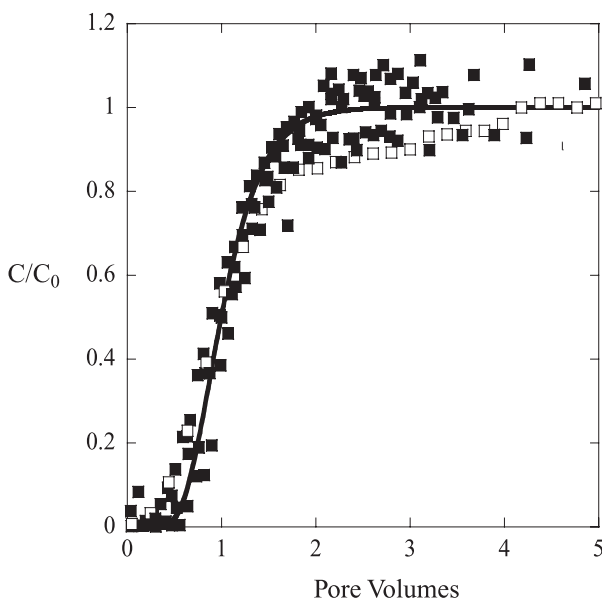

Fig. 2. Iodide breakthrough in column experiments at flow rate of 0.1 and 0.02 ml/min. Filled squares are for 1 M NaNO$_3$ experiments; unfilled squares are for the 5 M NaNO$_3$ experiment. Solid curve shows model result using a dispersivity of 1 cm.

Table 3
Selectivity coefficients, site concentrations, and effective equilibrium constants calculated based on batch binary exchange experiments (batch) and batch plus Cs^+ column experiments (column-weighted)

Exchange reaction	Batch, log K		Column-weighted, log K	
$NaX1 + Cs^+ = Na^+ + CsX1$	6.96		7.25	
$NaX2 + Cs^+ = Na^+ + CsX2$	3.64		4.93	
$NaX3 + Cs^+ = Na^+ + CsX3$	1.42		1.99	
$KX1 + Cs^+ = K^+ + CsX1$	4.81		4.99	
$KX2 + Cs^+ = K^+ + CsX2$	2.20		1.83	
$KX3 + Cs^+ = K^+ + CsX3$	0.72		0.74	
$0.5CaX1_2 + Cs^+ = 0.5Ca^{2+} + CsX1$	15.13		15.27	
$0.5CaX2_2 + Cs^+ = 0.5Ca^{2+} + CsX2$	8.94		10.89	
$0.5CaX3_2 + Cs^+ = 0.5Ca^{2+} + CsX3$	2.31		3.20	
$NaNO_3(aq) \rightarrow Na^+ + NO_3^-$	0.26		0.37	
$CsNO_3(aq) \rightarrow Cs^+ + NO_3^-$	0.49		0.47	
Ionic strength parameter (κ_{Cs-X})	−0.003		−0.136	

Exchange site	(μeq/g)	% of CEC	(μeq/g)	% of CEC
Site 1 (FES)	0.02	0.02	0.02	0.02
Site 2 (FES)	1.53	1.26	0.26	0.22
Site 3 (planar)	120	98.72	120	99.76
CEC	121.55		120.28	

a column with multiple regions with differing permeabilities and porosities. Capturing this behavior accurately would require some form of a multiregion modeling approach to describe transport in the column. Since the multiregion effect is relatively minor, it was decided to use a single region approach in the modeling.

4.3. Dependence of the Cs^+ K_d on Cs^+ and competing cation concentration

Results of the fitting of the batch exchange experiments and column-batch experiments are summarized in Table 3 and Fig. 3. The refitting of the batch data of Zachara et al.
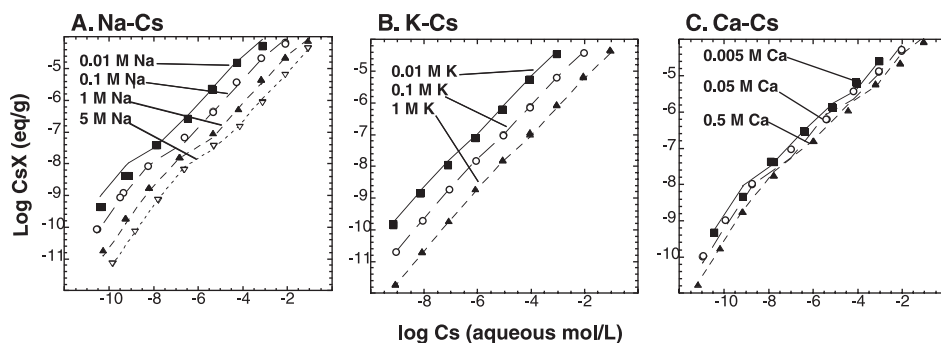

Fig. 3. Comparison of Cs^+ exchange on Hanford sediments measured in binary batch experiments (symbols) with cation exchange model (lines) derived from a global fit of selectivity coefficients and FES adsorption densities for all of the binary experiments. Batch data are from Zachara et al. (2002).

(2002) confirmed the strong variability of the cesium distribution coefficient (K_d) as a function of Cs^+ and competing cation concentration for Hanford sediments. The dependence of the Cs^+ K_d on the concentrations of the other cations (Na^+, K^+, and Ca^{2+}) is predicted quite well by the ion exchange theory (Fig. 3). Following Appelo and Postma (1993), we can rewrite Eq. (4) to obtain an expression for the Cs^+ K_d

$$K_d = CEC \frac{\beta_{Cs}}{[Cs^+]} = CEC \frac{1}{K_{M/Cs}} \frac{\beta_M^{1/m}}{[M^{m+}]^{1/m}}. \tag{8}$$

This classical expression of cation exchange indicates that the Cs^+ distribution coefficient cannot possibly be constant as a function of competing cation concentration. The observed nonlinearity of the Cs^+ K_d, however, is even stronger than what is expected based on this effect alone. The Cs^+ K_d in the case of the Hanford sediment also depends strongly on the Cs^+ concentration in solution, apparently because of the presence of multiple exchange sites with differing selectivities for Cs^+ vs. the other cations in the system. Fig. 4 shows the effect of both the competing Na^+ concentration (the most important background electrolyte at the SX tank farms at Hanford) and Cs^+ concentration on the Cs^+ K_d. If aqueous Cs^+ concentrations are less than or equal to the concentration of the frayed-edge sites (FES) with a high selectivity for Cs^+, then the K_d for Cs^+ will be correspondingly high. However, if the Cs^+ concentration significantly exceeds the concentration of FES, the K_d will be lower because the planar sites, despite being more abundant, have a lower selectivity for Cs^+. The strong curvature in the Cs^+ K_d surface at an aqueous Cs^+ concentration of about 10^{-6} M corresponds to the point where the aqueous
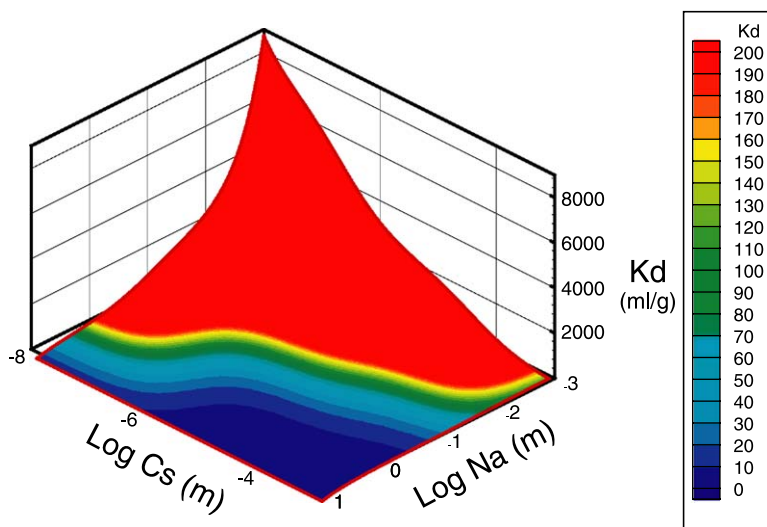

Fig. 4. Cs^+ distribution coefficient (K_d) as a function of aqueous Cs^+ and Na^+ concentration for sediments from the SX tank farm, Hanford. Based on a global fit (this paper) of binary exchange data from Zachara et al. (2002). Full range of the K_d (in units of ml/g) is 0–8000 as on surface plot—a narrower range of 0–200 is used in color bar for illustration purposes only.
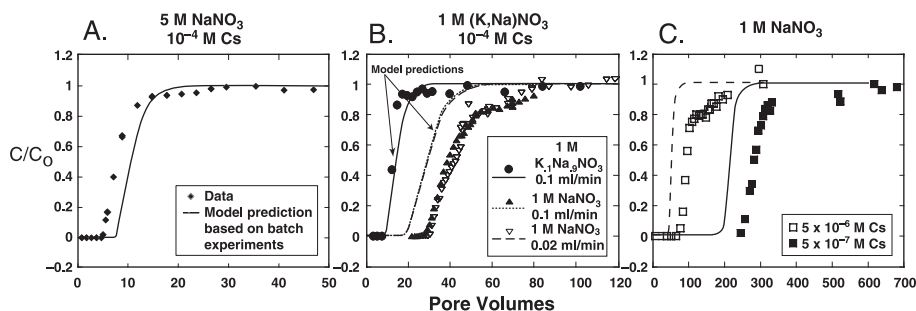
Fig. 5. Comparison of reactive transport simulations of Cs^+ breakthrough based on batch experiment-derived parameters (lines) with observed Cs^+ breakthrough (symbols).

Cs^+ concentration exceeds the adsorption density of the FES. Using K_d values calculated from the column-weighted fit results in a similar surface, although the values are generally shifted slightly higher relative to the batch fit. Note that the Cs^+ K_d is at a minimum where both the Cs^+ and Na^+ concentrations are highest. A more detailed discussion as to how batch and column-derived fits apply to the column experiments is given below.

4.4. Comparison of Cs^+ breakthroughs with model fits based on batch experiments

Reactive transport modeling based on parameters derived from binary batch experiments (Zachara et al., 2002) was used to predict Cs^+ retardation for flow-through column experiments carried out over a range of Cs^+ and salt concentrations (Fig. 5). The focus in this section is on a comparison of mean concentration breakthroughs of the Cs^+ ($C/C_0 = 0.5$). Discrepancies in the shape of breakthrough curves is discussed in Section 4.9. Retardation factors derived from the breakthrough of the mean Cs^+ concentration are summarized in Table 4. The batch-derived parameters slightly over-predict Cs^+ retardation in Hanford sediments when Na^+ or K^+ concentrations are high enough to compete strongly for exchange sites. For example, in 5 M $NaNO_3$ background electrolyte, retardation is about 8 in the experiment vs. a prediction of 10 by the model. A reasonably good match between model prediction and experiment in solutions containing K^+ (0.1 M KNO_3, 0.9 M $NaNO_3$, and 10^{-4} M Cs), yielding a Cs^+ retardation of about 12. In

Table 4
Cesium retardation in Hanford sediment for Cs^+ column experiments

Inlet salt solution	Inlet Cs (M)	Observed retardation	Model retardation batch fit	Model retardation column-weighted fit
5 M $NaNO_3$	10^{-4}	7.6	10.3	8.0
1 M $NaNO_3$	10^{-4}	42.7	29.3	40.2
1 M $NaNO_3$	10^{-4}	40.3	28.6	39.2
1 M $(Na_{0.9}K_{0.1})NO_3$	10^{-4}	12.6	14.0	11.0
1 M NaOH	10^{-4}	38.2	not available	45.6
1 M $NaNO_3$	5×10^{-6}	94.3	48.2	87.6
1 M $NaNO_3$	5×10^{-7}	282.2	215.8	271.0

contrast, Cs^+ retardation in the column experiments using the batch-derived parameters is under-predicted by as much as 25–55% at lower Na^+ and K^+ concentrations. In 1 M $NaNO_3$ experiments, Cs^+ retardation is about 41 at 10^{-4} M Cs^+, 94 at 5×10^{-6} M Cs^+, and 282 at 5×10^{-7} M Cs^+, compared to predicted retardations of 29, 48, and 215, respectively.

Some of the lack of agreement between the model predictions and Cs^+ retardation experiments appears to be the result of fitting over a very large range of both Cs^+ and Na^+ concentrations. On a logarithmic scale, small discrepancies between a model fit and a data point (usually 0.1 log unit or less) translate into easily discernable differences in the breakthrough time of Cs^+. We evaluated the effect of a slight misfit of the data in the global optimization of ion exchange parameters by weighting the batch exchange experiments at the $NaNO_3$ concentration corresponding to the conditions of the column experiment (e.g., 1 M $NaNO_3$ vs. 5 M $NaNO_3$) by a factor of 100. Weighting the data in this fashion improves slightly the match between the observed and calculated retardation, but it does not eliminate the discrepancies. The discrepancy between batch and column results, therefore, appears to be real. Fig. 6 shows a detail of the batch exchange results from Fig. 3a for the Cs^+–Na^+ system at 1 M $NaNO_3$ and Cs^+ concentrations close to 10^{-4} M. The observed retardations of 43 and 40 from the column experiments using 1 M $NaNO_3$ and 10^{-4} Cs (Table 4), along with the appropriate solid-solution ratios from Table 1, are used to calculate partitioning of Cs^+ between exchange sites and solution using Eq. (1). When the Cs^+ partitioning determined from the column experiments is compared to the Cs^+ partitioning observed in the binary batch exchange experiments, it is clear that the effective K_d for Cs is slightly higher (approximately 0.2 log units) in the columns than the batch experiments.
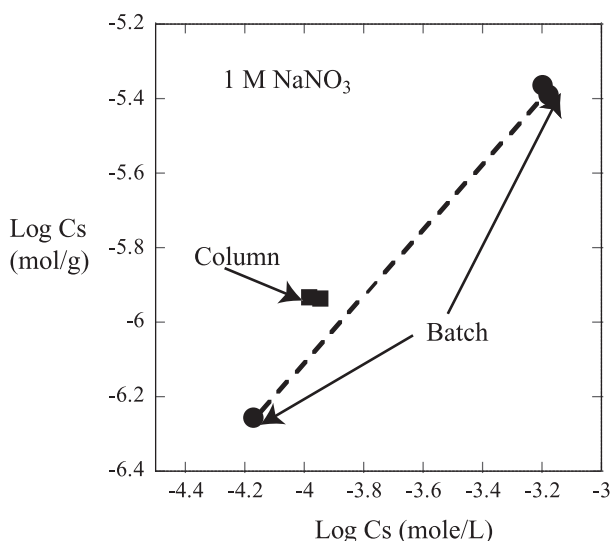

Fig. 6. Comparison of batch and column partitioning at 1 M $NaNO_3$.

4.5. Comparison of Cs$^+$ breakthroughs with model fits based on weighting of column data

To further evaluate the ion exchange model, we modified our Cs$^+$–Na$^+$–K$^+$–Ca^{2+} exchange model by fitting the selectivity coefficients and the cation exchange capacity with results from the column experiments weighted by a factor of 100 over the batch experimental data (Fig. 7 and Table 3). Batch experiments are included in the fitting procedure because the column experiments do not cover the entire range of cation concentrations of interest. The inclusion of the column-weighted data improves the match between predicted and observed cesium retardation in all of the Cs$^+$ transport experiments, with the effect most pronounced where the discrepancy between simulations based on batch-derived parameters and the data was greatest (experiments carried out in 1 M NaNO$_3$ and those using low Cs$^+$ injection concentrations). In general, the ion exchange parameters (site concentrations and selectivity coefficients) determined from the column-weighted fit result in predictions of greater Cs$^+$ retardation than the equivalent batch-derived parameters.

The experimental results and modeling present a compelling argument for the multisite, multicomponent ion exchange model used to describe Cs$^+$ transport. The very strong effect of competing cations can be seen in the case of both Na$^+$, the dominant cation at the SX tank farm (Fig. 7A and B) and K$^+$ (Fig. 7B), in agreement with classical ion exchange theory. In addition, the need for multiple sites of differing affinity for Cs$^+$ vs. the other cations is also clearly demonstrated in the column experiments. Reducing the Cs$^+$ injection concentration from 10^{-4} to 5×10^{-7} M results in a six-fold increase in the Cs$^+$ retardation (from 41 to 282), reflecting the higher selectivity of the frayed edge sites on micas (Sites 1 and 2) for Cs$^+$. Exchange at higher Cs$^+$ concentrations is likely to be dominated by the more abundant planar sites, which show a relatively weaker selectivity for Cs$^+$ compared to the other cations than do the FES.

4.6. Evidence for a three-site model from self-sharpened Cs$^+$ elution curves

A two-site model was proposed by Zachara et al. (2002) to describe Cs$^+$–Na$^+$, Cs$^+$–K$^+$, and Cs$^+$–Ca^{2+} binary exchange in sediments from the SX tank farm. In a
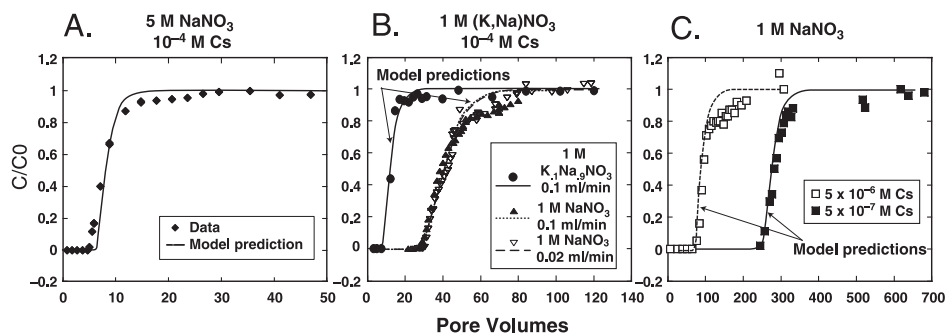

Fig. 7. Comparison of reactive transport simulations of Cs$^+$ breakthrough based on column-weighted fit of column and batch experiments (lines) with observed Cs$^+$ breakthrough (symbols).

global fit of these same binary exchange experiments, it was found that a three-site model provided a substantially better match of the $Cs^+–Ca^{2+}$ data and a slightly better match of the $Cs^+–Na^+$ data than did a two-site model. The two-site model, in contrast, was sufficient to match the $Cs^+–K^+$ binary exchange data remarkably well. Additional evidence supporting the applicability of a three-site model for Cs^+ exchange comes from the geometry of Cs^+ elution curves at various inlet concentrations of Cs^+. In the absence of reaction, the shape of a breakthrough curve is controlled by the magnitude of the dispersivity for the sediment in the column. This was determined to be 1 cm based on matches of iodide breakthrough curves in all the experiments (Fig. 2). Elution curves for reactive species may be "self-sharpened", however, as a result of stronger sorption of the eluted species at low concentrations than at high concentrations (Appelo and Postma, 1993; Appelo, 1996). The two-site model, while it correctly predicts the retardation at a C/C_0 of 0.5, does not capture the steep breakthrough curve shown by the experimental data at a Cs^+ injection concentration of 5×10^{-7} M (Fig. 8). The three-site model, because it produces a relatively strong change in retardation over the concentration range of Cs^+ in the experiment (about 5×10^{-8} to 5×10^{-7} M), captures the self-sharpening of the Cs^+ breakthrough curve.

Brouwer et al. (1983) and Cremers et al. (1988) both presented evidence for the existence of a third type of exchange site based on an improved ability to match adsorption isotherms for illite clay. In contrast, Poinssot et al. (1999) argued that only two sites were required based on their data on illite. Zachara et al. (2002) also argued that only two sites were necessary to describe the binary batch exchange data on the Hanford composite sediment (the same data set that was used in fits based on batch experiments in this study). They determined an FES concentration of $2.72–3.45 \times 10^{-8}$ eq/g based on multisite modeling assuming the presence of two sites. Zachara et al. (2002) also carried out a
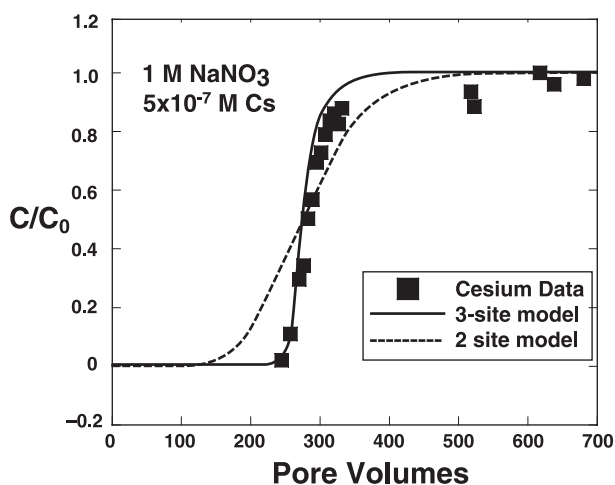

Fig. 8. Comparison of model fit of Cs^+ breakthrough curve using two and three site models. The three-site model captures the self-sharpened breakthrough curve resulting from the higher Cs^+ retardation at low Cs^+ concentration. The two-site model, in contrast, produces a breakthrough geometry controlled by dispersion.

limited number of experiments using AgTU (silver thiourea) as an agent for blocking planar sites on expansible clays following the approach of Cremers et al. (1988) and De Preter et al. (1991). Using the AgTU blocking procedure, Zachara et al. (2002) determined an operationally defined FES concentration of 7.94×10^{-7} eq/g (about 1.86% of the total CEC that they measured), well above the adsorption density of about 3×10^{-8} eq/g determined from multisite modeling for Site 1. Zachara et al. (2002) also noted a very clear change in slope in a plot of the conditional equilibrium constant (K_c) at an adsorption density of 4×10^{-8} eq/g (their Fig. 11B), indicating a strong change in the selectivity for Cs^+ at this adsorption density. The global refit of the batch data presented in this study also provides support for the existence of a discrete site with a very high selectivity for Cs^+ (Site 1) at a sorption density of about 2.4×10^{-8} eq/g, or about 0.02% of the total CEC (Table 3). The existence of this site is clear. Less clear, however, is whether evidence exists for a second FES site with a higher adsorption density. Zachara et al. (2002) argued that the AgTU was ineffective in blocking all planar sites and that therefore the higher adsorption density determined by the AgTU method should be viewed with caution. Another possible interpretation, however, is that the FES determination based on the AgTU blocking procedure is real and that it represents a second type of FES site with a relatively lower selectivity for Cs^+ than FES Site 1. Note that the FES adsorption density determined by Zachara et al. (2002) with the AgTU blocking procedure is close to that determined in this study for Site 2 using the combined batch and column experiments (Table 3).

It should also be noted that conclusions as to the number of sites present may depend on the particular binary system considered—for example, the Cs^+–K^+ binary data do not require a third site, while data from the Cs^+–Na^+ and Cs^+–Ca^{2+} experiments suggest an improved fit can be obtained when a second FES site is included. Brouwer et al. (1983) based much of their argument for the existence of three sites on a comparison of Rb^+ and Cs^+ sorption. They demonstrated that, at vanishly small loadings of Cs^+ or Rb^+, the illite clay showed a pronounced selectivity for Cs^+ over Rb^+. At intermediate loadings, no selectivity for either cation could be detected, while at high loadings (where planar sites presumably dominated), the clay again showed a preference for Cs^+ over Rb^+. The most sensitive technique for determining the correct number of sites and their adsorption densities may be to consider multiple cations with differing selectivities for the exchangers.

Another point that may be relevant in terms of the discussion over the number of distinct exchange sites necessary to describe Cs^+ sorption on Hanford sediment is that ultimately only a single set of site concentrations can be used if the intent is to apply the model to a real system. For example, both Brouwer et al. (1983) and Zachara et al. (2002) reported FES adsorption densities that varied depending on whether the Cs^+–K^+ or the Cs^+–Na^+ system was considered. While these differing adsorption densities might apply where the exchangers are completely saturated with a single dominant cation (K^+ or Na^+), clearly both adsorption site densities cannot be used in a multicomponent Cs^+–Na^+–K^+ system where all cations compete for the same site or sites. It may be that the use of conflicting adsorption site densities for different binary systems biases the results so as to favor a model based on a lesser number of distinct sorption sites.

4.7. Effect of K^+ on Cs^+ exchange

Potassium enhances the mobility of Cs^+ because it has a higher affinity for the exchange sites on micas and clays than do either Na^+ or Ca^{2+} (Table 3). Since the tank wastes contain elevated concentrations of K^+ as well as Na^+, we conducted an exchange experiment in the K^+–Cs^+–Na^+ system to further test the ion exchange model. Another source of K^+ in the contaminant plume is from the dissolution of mica and feldspar minerals in the highly alkaline and elevated temperature waste stream. Fig. 7B compares the column transport behavior of Cs^+ in binary (Cs^+–Na^+) and ternary (K^+–Cs^+–Na^+) electrolyte systems. The initial Cs^+ concentration (10^{-4} M) and total salt concentration (1 M) are the same in both experiments. In solutions containing 0.1 M KNO_3 and 0.9 M $NaNO_3$, Cs^+ retardation is about one-third of what it is in 1 M $NaNO_3$, in agreement with the model prediction.

4.8. Cs^+ exchange in alkaline solutions

It is important to establish whether the multi-cation Cs^+ exchange model can be extrapolated to the alkaline conditions reported in the S-SX tank farm wastes. While pH does not have a direct effect on Cs^+ exchange, except at low pH conditions where the hydrogen ion can compete directly for exchange sites (Poinssot et al., 1999), it can have an indirect effect through aqueous complexation or mineral dissolution. In the nitrate-dominated system considered here, the pH dependence of complexation is minor, with only weak formation of the ion pairs $CsOH_{aq}$ and $NaOH_{aq}$. Mineral dissolution and precipitation reactions, however, can affect Cs^+ mobility by altering the number and distribution of sites and by providing a source for dissolved K^+ that competes for Cs^+ exchange.

Fig. 9 compares Cs^+ elution curves and model predictions from a single 1 M NaOH experiment (pH 13.7) and the 1 M $NaNO_3$ experiments (pH 8), both of which used a Cs^+ injection concentration of 10^{-4} M. Cesium retardation based on the breakthrough of the half-concentration ($C/C_0 = 0.5$) is slightly over predicted in the 1 M NaOH experiments by
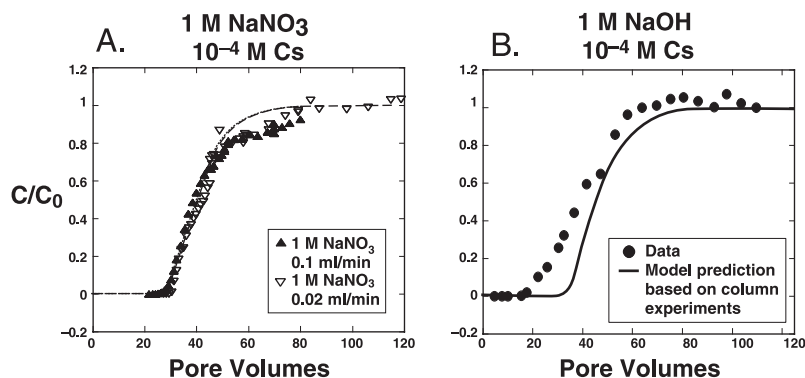

Fig. 9. Comparison of Cs^+ breakthrough in 1 M NaOH with breakthrough in 1 M $NaNO_3$ at circumneutral pH.

about 10–15%. In addition, the initial breakthrough of Cs^+ in the experiment is earlier than is predicted by the model. The results of the high base Cs^+ elution experiments suggest that the model might be extended in an approximate fashion to the alkaline tank waste, although more experiments would be needed to improve the accuracy under these conditions.

The model used in Fig. 9B incorporated the measured OH^- and K^+ (1.5×10^{-4} M) concentrations at steady state, but did not explicitly account for mineral dissolution or precipitation. About 4 wt.% of the sediment dissolved based on the composition of the output solutions. During the first few hours of reaction, there was rapid mineral dissolution and re-precipitation in the sediments. SEM and EDS analyses of the sediments at the end of the experiment revealed a precipitate that was rich in silica, Fe, Mg, and Ca (not shown here). This precipitate is probably amorphous, since it was not detected by X-ray diffraction (D. Bish, personal communication).

4.9. Discontinuities in Cs^+ breakthrough: a kinetic or multicomponent equilibrium effect?

When Cs^+ concentrations during breakthrough reach about 75–85% of the inlet concentration, the relatively steep Cs^+ breakthrough curve changes to a much more gradual one. This is in contrast to the equilibrium model results that rapidly approach a C/C_0 of 1.0 (Fig. 7B and C). As noted above, the non-reactive tracer I^- also shows a discontinuity in the its breakthrough curve close to $C/C_0 = 1.0$, probably as a result of slow diffusion into low porosity subdomains within the column. The effect with Cs^+, however, is much more pronounced than it is with the non-reactive tracer, particularly in experiments run at lower Cs^+ injection concentrations where the effect may be seen over hundreds of pore volumes (Fig. 7C). The long gradual approach to the injection concentration of Cs^+ may indicate a rate limitation on Cs^+ uptake (Saiers and Hornberger, 1996), perhaps as a result of slow diffusion into intralamellar sites in micas (Lomenick and Tamura, 1965; Klobe and Gast, 1970; Le Roux et al., 1970; Comans et al., 1991; Smith and Comans, 1996). According to this interpretation, the shape of the iodide and Cs^+ breakthrough curves might be similar because both result from slow diffusion-controlled exchange, with the non-reactive iodide curve reflecting intergranular diffusion into low porosity subdomains and the Cs^+ curve reflecting intralamellar diffusion within micas.

As an alternative explanation, the change in slope in the Cs^+ breakthrough curve may be the result of multicomponent effects, for example, the desorption of K^+ from exchange sites by Cs^+. Modeling of the $NaNO_3$ pre-flush stage suggests that K^+ should be quantitatively removed from even the FES, since the selectivity coefficient for the Na^+–K^+ exchange reaction is about $10^{2.25}$. However, there may be a kinetic limitation to the desorption of K^+ by Na^+. Some support for this interpretation was provided by Cs^+ and K^+ data collected in the experiment using 5×10^{-6} M Cs^+ and 1 M $NaNO_3$ and plotted in Fig. 10. This experiment follows a pre-flushing stage (without CsI) in which a 1 M KNO_3 flush was followed with a 1 M $NaNO_3$ flush lasting over 50 pore volumes. Equilibrium modeling in this case would predict that the K^+ concentration on exchangers and in solution should be well below 10^{-10} M, but actual K^+ concentrations measured are close to 10^{-3} M. In advance of the Cs^+ breakthrough (Fig. 10), K^+ concentrations are declining until a distinct jump in K^+ concentration occurs immediately before the arrival of the Cs^+ front. This would appear to represent K^+ desorbed from exchange sites in the sediment by Cs^+. It is possible
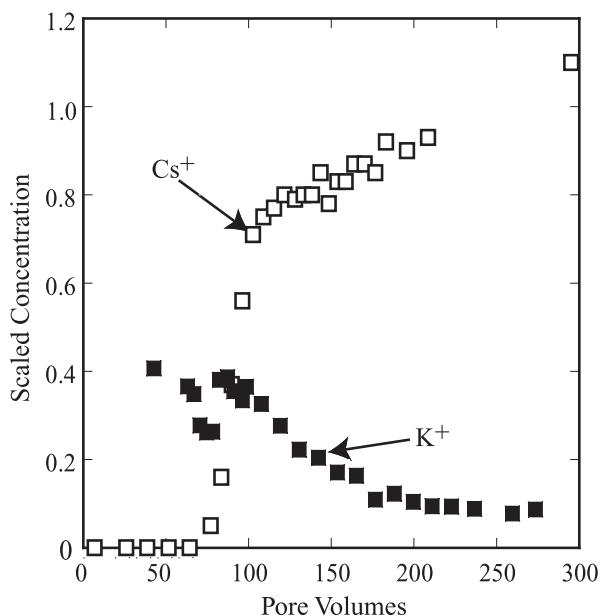
Fig. 10. Detail of Cs^+ and K^+ elution in experiment using 5×10^{-6} M Cs^+ and 1 M $NaNO_3$. Cs^+ concentration has been divided by the inlet concentration of 5×10^{-6} M, while K^+ has been scaled by 10^{-3}.

that the Cs^+ breakthrough curve becomes more gradual as a result of the slow desorption of K^+ from FES once the distinct K^+ front has passed. Like the kinetic explanation discussed above, this multicomponent effect is not captured by the modeling.

4.10. Reversibility of Cs^+ exchange

Assessing the reversibility of Cs^+ exchange is crucial for predicting its future mobility. Measurements of Cs^+ desorption from contaminated S-SX sediments at Hanford (41-09-39 and SX-108) suggest partial fixation of the sorbed Cs pool (McKinley et al., 2001). The reversibility of Cs^+ exchange was examined by following the sorption stage with a desorption stage using an identical injection solution except for the absence of CsI. Fig. 11 shows Cs^+ sorption and desorption for four experiments carried out with 10^{-4} M Cs^+ and 5 M $NaNO_3$, 5×10^{-6} M Cs^+ and 1 M $NaNO_3$, 5×10^{-7} M Cs^+ and 1 M $NaNO_3$, and 10^{-4} M Cs^+ and 1 M NaOH, along with their respective model predictions based on the column-weighted parameters. Column experiments conducted at Cs^+ injection concentrations of 5×10^{-6} and 5×10^{-7} M, and 1 M $NaNO_3$ were specifically designed to test the reversibility of Cs^+ exchange on FES, since under these conditions exchange on planar sites is minimal. These Cs^+ transport experiments show the strongest evidence for slow uptake of Cs^+ into exchange sites, although it is not clear whether this is a kinetic effect related to slow diffusion into intralamellar sites in micas (e.g., Comans et al., 1991) or to multicomponent equilibrium effects (e.g., the desorption of K^+) as discussed above.
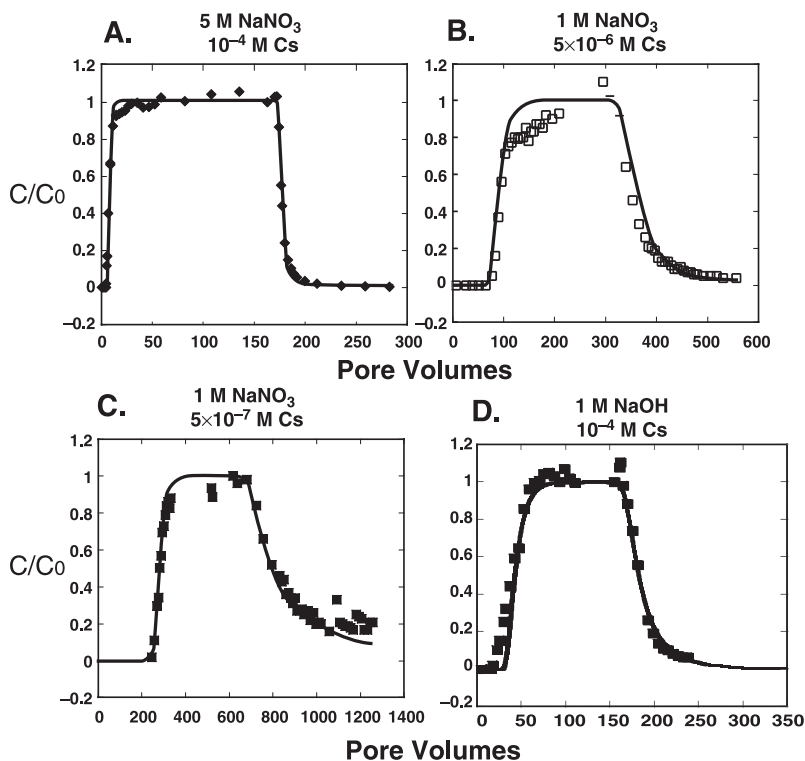
Fig. 11. Reversibility of Cs^+ exchange, with equilibrium reactive transport model results based on column-weighted parameters to observed Cs^+ elution.

In the desorption experiments, mass balance calculations indicate that 72% and 87% of the original Cs sorbed in the 5×10^{-6} and 5×10^{-7} M Cs^+ experiments respectively were desorbed by elution with 1 M $NaNO_3$. Based on the fact that the equilibrium modeling captures quite well the shape and actual concentrations of Cs^+ during desorption, it appears that the slow desorption of Cs^+ is primarily the result of the extremely high selectivity of the FES for Cs^+ vs. Na^+. The slow desorption of Cs^+, therefore, would appear to be an equilibrium effect and mostly reversible in the thermodynamic sense. Slow diffusion-controlled release of Cs^+, however, cannot be ruled out as a contributor to this effect, since it may be masked by the very long times required to desorb Cs^+ even under equilibrium conditions. The equilibrium modeling predicts that about 300 pore volumes of elution with 1 M $NaNO_3$ is required to desorb 95% of the total Cs^+ sorbed in the 5×10^{-6} M Cs experiment (Fig. 11B). The difference between the 72% value actually measured and the 95% predicted by the equilibrium model is primarily the result of the extra mass of Cs^+ sorbed on the Hanford sediment during the Cs^+ uptake stage that was not captured by the modeling. It might be argued, therefore, that this 23% of the total Cs^+ sorbed in this experiment is irreversibly sorbed.

In experiments using higher injection concentrations of Cs^+ and where exchange is therefore controlled primarily by sorption to planar sites, there is less evidence for

irreversible Cs^+ uptake. Presumably, irreversible sorption on FES might occur, but the effect might not be apparent against the background of higher Cs^+ input and output concentrations in these experiments. The Cs^+ elution curve at 10^{-4} Cs and 5 M $NaNO_3$ (Fig. 11A) and 1 M NaOH (Fig. 11D) show the closest agreement with the equilibrium exchange model, with only a minor discrepancy observed at Cs^+ elution concentrations within 90% of the injection concentration. Mass balance calculations indicate that 95% of the originally exchanged Cs^+ was desorbed.

4.11. Batch–column discrepancies

The source of the discrepancy between predictions of Cs^+ retardation based on batch- and column-derived data is not clear given the available information. One possible explanation for these discrepancies is based on the interpretation that the mismatch between Cs^+ breakthrough curves during the sorption stage (Fig. 7B and C) is attributable to slow diffusion-controlled uptake of Cs^+, and not to a multicomponent equilibrium effect (e.g., the desorption of K^+) as discussed. To test this hypothesis, we calculate the mass and rate of Cs^+ incorporation into slowly exchanging sites by subtracting the integrated area under the model (equilibrium) Cs^+ elution curve from the integrated area under the observed Cs^+ elution curve. For example, in the experiment using a Cs^+ injection concentration of 5×10^{-7} M (Fig. 7C), the discrepancy between the model and the data between 250 and 680 pore volumes suggests the sorption of 7×10^{-8} total moles of Cs^+ to slowly exchanging sites. Assuming the rate of Cs^+ incorporation into slowly exchanging sites determined after Cs^+ breakthrough applies to the period prior to breakthrough (when any hypothesized kinetic effects are not apparent), it is possible to estimate the decrease in sorbed Cs^+ retardation in the absence of this rate-limited exchange. A calculation of the increase in retardation predicted using batch-derived parameters is less straightforward, since the integration time to break-through is a priori unknown. The calculations suggest about 7.2% of the Cs^+ is slowly exchanging in the 5×10^{-7} M Cs^+ experiment prior to Cs^+ breakthrough and as much as 18.2% over the entire experiment. Applying the adjustment to the Cs^+ mass sorbed prior to Cs^+ breakthrough suggests an equivalent reduction in Cs^+ retardation of 7.2% to 262 from 282, a value slightly closer to the value of 216 predicted using the batch-derived parameters. Calculations using data from other experiments show similar small reduc-tions in the predicted Cs^+ retardation, although in each case the adjustment is not enough to match the observed discrepancy.

Other explanations for the discrepancy between batch- and column-derived parameters are possible. The high concentrations of K^+ in the column effluent in the 5×10^{-6} M Cs^+ experiment suggest that it may difficult to remove all of the various cations originally present on exchange sites. Batch experiments designed to evaluate the Na^+–Cs^+ system, therefore, may not have been true binary experiments, since small amounts of K^+ desorbed from exchange sites could result in lower Cs^+ sorption. This would have the effect of lowering the effective Cs^+ K_d relative to what would be expected in a true binary system. The column experiments, which rely on flushing of the sediment with many pore volumes, should be more effectively in flushing the competing K^+, Ca^{2+}, and Mg^{2+} out of the sediment than would a batch experiment.

Other studies have noted a discrepancy between batch and column results in the case of Cs^+, with column experiments showing greater retardation of Cs (Schmalz, 1972; Reynolds et al., 1982). In the study by Reynolds et al. (1982), Cs distribution coefficients were as much as 2.1 times greater in column experiments than in the batch study, despite their use of identical solution compositions. Schmalz (1972) reported a column-determined K_d, which was 3.5 times greater than the batch-determined value.

5. Implications for cesium migration at Hanford SX tank farm

5.1. Enhanced Cs^+ migration below leaking SX tanks

One of the most significant implications of this work is the confirmation that the Cs^+ distribution coefficient (K_d) is not constant over the range of Na^+, K^+, Ca^{2+}, and Cs^+ concentrations found in the tank farm inventory and in the vadose zone pore water at the S-SX tank farm. A constant K_d can be used in describing Cs^+ migration below leaking tanks at Hanford only when the leak rate and its composition are constant and no dilution or concentration of the plume occurs. Even in this case, the value of the K_d depends on the composition of the tank leak. Any process that acts to change either the leak rate or its composition, including dilution due to mixing or concentration due to evaporation or boiling, will cause the Cs^+ K_d to vary in time and space. A tank leak rate which varies or is short-lived will always result in a spatially and temporally variable K_d in the case of ion exchange, since the natural chromatographic separation of competing cations causes the retardation of Cs^+ to increase.

The following example shows that the multisite cation exchange model describes Cs^+ retardation that is at least qualitatively consistent with ^{137}Cs observations at the SX tank farm. A detailed, quantitative analysis of Cs^+ migration at the SX tank farm is the subject of a future contribution. Our column experiments indicate that high competing cation concentrations associated either with the tank liquors or resulting from reactions in the sediment underlying the tank cause a significant decrease in the retardation of Cs^+. The SX-115 tank leak apparently contained between about 1 M and 3 M $NaNO_3$ and 2.2×10^{-5} and 8×10^{-5} M Cs^+ (Lichtner, 2001; Steefel and Yabusaki, 2001). Our model for Cs^+ exchange predicts a retardation of about 11 prior to any dilution of the tank liquors by vadose zone processes. This agrees qualitatively with the strong retardation of Cs^+ observed below SX-115. In addition, some retardation of Na^+ is expected at these $NaNO_3$ concentrations, a prediction which is in qualitative agreement with observations made in bore hole WB 23-19 where Na^+ peaks lag behind NO_3^- peaks (Serne et al., 2001a). In contrast, leaking tank liquors at SX-108 were at or above the boiling temperature and were extremely concentrated, with some estimates giving $NaNO_3$ concentrations at or close to equilibrium with respect to solid $NaNO_3$ (about 17 molal Na^+ at 100 °C according to Lichtner, 2001) and 7×10^{-4} M Cs^+. At these very high $NaNO_3$ concentrations, one does not expect to see any retardation of Na^+, in agreement with field observations that show that Na peaks are coincident with nitrate peaks (Serne et al., 2001b). One also expects significantly less retardation of Cs^+ at these extremely high $NaNO_3$ concentrations. Extrapolating the column-weighted fits of Cs^+ exchange to 15 M

$NaNO_3$ yields a predicted Cs^+ retardation factor of between 2 and 3. This value is close to the observed retardation of Cs^+ below the SX-108 tank (Serne et al., 2001b). While this prediction is uncertain without direct experimental confirmation of Cs^+ retardation at these $NaNO_3$ concentrations and at higher temperature and without detailed thermal–hydro-logical–chemical modeling of the SX-108 tank leak, the ion exchange model presented here suggests that the high $NaNO_3$ concentrations may account for the bulk of the enhanced Cs^+ mobility observed at Hanford.

5.2. Implications for future mobility of Cs^+

It is tempting, based on the small retardation of Cs^+ below the SX-108 tank leak, to conclude that Cs^+ could migrate further in the future at this site. The multisite, multi-component model developed here, however, suggests a more complicated but ultimately favorable conclusion. The original enhanced migration of Cs^+ below the SX-108 tank is apparently the result of the very high salt concentrations and elevated temperatures. Under these conditions, Cs^+ sorption on planar sites will be suppressed, so Cs^+ will tend to migrate until all of the available Cs^+ is sorbed by high selectivity FES only. This region is necessarily much larger than would be the case if sorption occurred also on the abundant planar sites since the FES are present in relatively low concentrations. With the return of natural recharge, however, there will be little tendency to displace Cs^+ from the high selectivity FES, particularly since seepage water will tend to be much more dilute than was the case with the tank leak solutions. Although this study does not suggest that Cs^+ sorption is fundamentally irreversible in a thermodynamic sense, the very high affinity of the FES for Cs^+ (recall that the selectivity coefficient for Na^+–Cs^+ is about 10^7) suggests that a very large number of pore volumes of dilute recharge water would be required to mobilize the Cs^+ further. The Cs^+ below the SX-108 tank, therefore, could be considered as immobile.

6. Conclusions

The multicomponent exchange model captures much of the chemistry responsible for the dependence of the Cs^+ K_d on competing cation and Cs^+ concentrations and is a significant improvement over the use of a constant K_d to model Cs^+ from tank leaks to the vadose zone sediments. The experimental evidence and reactive transport modeling support a multisite exchange model based on three distinct exchange sites with differing affinities for Cs^+ and adsorption densities. We conclude that two distinct FES account for 0.02% and 0.2% of the total CEC and that these sites have Na^+–Cs^+ selectivities of $10^{7.25}$ and $10^{4.93}$, respectively. A third site related to surfaces on expansible clays ("planar sites") accounts for over 99% of the cation exchange capacity of the sediment and shows a Na^+–Cs^+ selectivity coefficient of 10^2. While Zachara et al. (2002) proposed a two-site model for Cs^+ exchange, a third site was invoked in this study to improve the fit of the Cs^+–Ca^{2+} and Cs^+–Na^+ binary exchange data and to capture the shape of self-sharpened Cs^+ break-through curves at low concentrations of Cs^+ in the feed solution. Modeling of Cs^+ migration using batch-derived exchange parameters under predicts actual Cs^+ retardation in the columns in most cases. The under prediction of Cs^+ retardation, however, was remedied by

carrying out a global fit that combined batch data with results of the column elution experiments. The fit of both column and batch data was based on independent determination of the total CEC of the Hanford sediment using ^{22}Na isotopic equilibrium exchange in an elution experiment. The value for the CEC of 120 μeq/g determined with this method is compatible with a determination of 121.9 μeq/g based on multi-cation elution.

The experimental results, combined with equilibrium reactive transport modeling, indicate that Cs^+ exchange is largely reversible on the Hanford sediments over time scales up to six weeks. For example, in a column experiment targeting Cs^+ sorption on FES using 5×10^{-7} M Cs^+ and 1 M $NaNO_3$, 87% of the Cs^+ sorbed was eventually desorbed by the end of the 6-week period. Equilibrium reactive transport modeling, however, predicted that the desorption of Cs^+ should not yet be complete even after this period because of the very high selectivity of the FES for Cs^+ in $NaNO_3$ solutions. The conclusion is that, while Cs^+ is reversibly sorbed in the thermodynamic sense, it can be viewed operationally as being immobile because of the hundreds to even thousands of pore volumes required to desorb it when exchange occurs on FES.

The non-constancy of the Cs^+ distribution coefficient over the range of Na^+, K^+, Ca^{2+}, and Cs^+ concentrations found in the tank farm inventory has important implications for modeling of Cs^+ transport in the vadose zone at the S-SX tank farm. Very substantial decreases in Cs^+ retardation are possible where very concentrated $NaNO_3$ plumes develop, as may be the case with tanks that have undergone boiling prior to leaking. Other tank leaks, which consisted of more dilute salt solutions, are expected to show significantly greater Cs^+ retardation. Other processes, such as dilution and evaporation, and the natural chromatographic separation of cations which occurs when the tank leak rate varies or is short-lived, all contribute to a spatially and temporally variable Cs^+ distribution coefficient.

References

AntonopoulosDomis, M., Clouvas, A., Hiladakis, A., Kadi, S., 1995. Radiocesium distribution in undisturbed soil-measurements and diffusion–advection model. Health Physics 69, 949–953.

AntonopoulosDomis, M., Clouvas, A., Xanthos, S., Alifrangis, D.A., 1997. Radiocesium contamination in a sub-Mediterranean semi-natural ecosystem following the Chernobyl accident: measurements and models. Health Physics 72, 243–255.

Appelo, C.A.J., 1994. Some calculations on multicomponent transport with cation-exchange in aquifers. Ground Water 32, 968–975.

Appelo, C.A.J., 1996. Multicomponent ion exchange and chromatography in natural systems. In: Lichtner, P.C., Steefel, C.I., Oelkers, E.H. (Eds.), Reactive Transport in Porous Media. Reviews in Mineralogy, vol. 34, pp. 193–227.

Appelo, C.A.J., Postma, D., 1993. Geochemistry, Groundwater, and Pollution. A.A. Balkema, Rotterdam.

Appelo, C.A.J., Willemsen, A., 1987. Geochemical calculations and observations on salt water intrusions, I. Journal of Hydrology 94, 313–330.

Appelo, C.A.J., Willemsen, A., Beekman, H.E., Griffioen, J., 1990. Geochemical calculations and observations on salt water intrusions, II. Journal of Hydrology 120, 225–250.

Appelo, C.A.J., Hendrick, J.A., van Veldhuizen, M., 1993. Flushing factors and a sharp front solution for solute transport with multicomponent ion exchange. Journal of Hydrology 146, 89–113.

Bond, W.J., 1997. Competitive exchange of K^+, Na^+, and Ca^{2+} during transport through soil. Australian Journal Soil Research 35, 739–752.

Brouwer, E., Baeyens, B., Maes, A., Cremers, A., 1983. Cesium and rubidium ion equilibria in illite clay. Journal of Physical Chemistry 87, 1213–1219.

Celia, M.A., Gray, W.G., 1992. Numerical Methods for Differential Equations: Fundamental Concepts for Scientific and Engineering Applications. Prentice-Hall, Englewood Cliffs, NJ.

Cernik, M., Borkovec, M., Westall, J.C., 1996. Affinity distribution description of competitive ion binding to heterogeneous materials. Langmuir 12, 6127–6137.

Charbeneau, R.J., 1988. Multicomponent exchange and subsurface solute transport: characteristics, coherence and the Reimann problem. Water Resources Research 24, 57–64.

Chibowski, S., Zygmunt, J., Klimowiz, Z., 1999. Investigation of adsorption and vertical migration of Cs-137 in three kinds of soil at Lublin vicinity. Journal of Radioanalytical and Nuclear Chemistry 242, 287–295.

Comans, R.N., Haller, J.M., De Preter, P., 1991. Sorption of cesium on illite: non-equilibrium behavior and reversibility. Geochimica et Cosmochimica Acta 55, 433–440.

Cremers, A., Elsen, A., De Preter, P., Maes, A., 1988. Quantitative analysis of radiocesium retention in soils. Nature 335, 247–249.

Datta-Gupta, A., Lake, L., Pope, G., Sepehrnoori, K., King, M., 1991. High-resolution monotonic schemes for reservoir flow simulation. In Situ 15, 289–317.

De Preter, P., Van Loon, L., Maes, A., Cremers, A., 1991. Solid/liquid distribution of radiocesium in boom clays: a quantitative interpretation. Radiochimica Acta 52/53, 299–302.

Doherty, J., Lindsay, B., Whyte, P., 1994. PEST: Model Independent Parameter Estimation. Watermark Computing, Brisbane, Australia.

Felmy, A.R., 1995. GMIN, a computerized chemical equilibrium program using a constrained minimization of the Gibbs free energy: summary report. Chemical Equilibrium and Reaction Models. Soil Science Society of America, Madison, WI.

Francis, C.W., Brinkley, F.S., 1976. Preferential adsorption of ^{137}Cs to micaceous minerals in contaminated freshwater sediment. Nature 260, 511–513.

Giani, L., Helmers, H., 1997. Migration of cesium-137 in typical soils of north Germany ten years after the Chernobyl accident. Zeitschrift fur Pflanzenernahrung und Bodenkunde 160, 81–83.

Griffioen, J., Appelo, C.A.J., van Veldhuizen, M., 1992. Practice of chromatography: deriving isotherms from elution curves. Soil Science Society of America Journal 56, 1429–1437.

Guttierrez, M., Fuentes, H.R., 1993. Modeling adsorption in multicomponent systems using a Freundlich-type isotherm. Journal of Contaminant Hydrology 14, 247–260.

Jackson, M.L., 1963. Interlaying of expansible layer silicates in soils by chemical weathering. Clays and Clay Minerals 11, 29–46.

Kemner, K.M., Hunter, D.B., Bertsch, P.M., Kirkland, J.P., Elam, W.T., 1997. Determination of the site-specific binding environments of surface sorbed cesium on clay minerals by Cs-EXAFS. Journal de Physique, IV France 7, 777–779.

Klobe, W.D., Gast, R.G., 1970. Conditions affecting cesium fixation and sodium entrapment in hydrobiotite and vermiculite. Soil Science Society of America Proceedings 34, 746–750.

Klyashtorin, A.L., Shcheglov, A.I., Tsvetnova, O.B., 1999. Vertical migration of Cs-137 in pine forest biogeocenoses. Eurasian Soil Science 32, 1347–1351.

Le Roux, J., Rich, C.I., Ribbe, P.H., 1970. Ion selectivity by weathered micas as determined by microprobe analysis. Clays and Clay Minerals 18, 333–338.

Lichtner, P.C., 2001. Estimating tank supernatant liquid composition and reactive flow and transport sensitivity analyses. PNNL-2001-7, Pacific Northwest National Laboratory, Richland, WA.

Lomenick, T.F., Tamura, T., 1965. Naturally occurring fixation of ^{137}Cs on sediments of lacustrine origin. Soil Science Society of America Proceedings 29, 383–387.

McKinley, J.P., Serne, R.J., Zachara, J.M., Zeissler, C.J., Lindstrom, R.M., 2001. The distribution and retention of ^{137}Cs in sediments beneath leaked waste at the Hanford site. Environmental Science and Technology 35, 3433–3441.

Parkhurst, D.L., 1995. User's guide to PHREEQC—a computer program for speciation, reaction-path, advective transport, and inverse geochemical calculations. U.S. Geol. Survey Water Resource Invest. Report, Denver, CO, 95–4227.

Poinssot, C., Baeyens, B., Bradbury, M.H., 1999. Experimental and modeling studies of cesium sorption on illite. Geochimica et Cosmochimica Acta 63, 3217–3227.

Rafferty, B., Brennan, M., Dawson, D., Dowding, D., 2000. Mechanisms of Cs-137 migration in coniferous forest soils. Journal of Environmental Radioactivity 48, 131–143.

Reynolds, W.D., Gillham, R.W., Cherry, J.A., 1982. Evaluation of distribution coefficients for prediction of strontium and cesium migration in a uniform sand. Canadian Geotechnical Journal 19, 92–103.

Rich, C.I., Black, W.R., 1964. Potassium exchange as affected by cation size, pH, and mineral structure. Soil Science 97, 384–390.

Saiers, J.E., Hornberger, G.M., 1996. Migration of ^{137}Cs through quartz sand: experimental results and modeling approaches. Journal of Contaminant Hydrology 22, 255–270.

Sawhney, B.L., 1970. Potassium and cesium ion selectivity in relation to clay mineral structure. Clays and Clay Minerals 18, 47–52.

Schmalz, B.L., 1972. Radionuclide distribution in soil mantle of the lithosphere as a consequence of waste disposal at the National Reactor Testing Station. U.S. Atomic Energy Commission, Report IDO-10049, Washington, DC.

Serne, R.J., Schaef, H.T., Bjornstad, B.N., Lanigan, D.C., Gee, G.W., Lindenmeier, C.W., Clayton, R.E., LeGore, V.L., O'Hara, M.J., Brown, C.F., Orr, R.D., Last, G.V., Kutnyakov, I.V., Burke, D.B., Wilson, T.C., Williams, B.A., 2001a. Geologic and geochemical data collected from vadose zone sediments from borehole 299 W23-19 [SX-115] in the S/SX Waste Management Area and Preliminary Interpretations. PNNL-2001-3, Pacific Northwest National Laboratory, Richland, WA.

Serne, R.J., Schaef, H.T., Last, G.V., Lanigan, D.C., Lindenmeier, C.W., Clayton, R.E., LeGore, V.L., O'Hara, M.J., Brown, C.F., Orr, R.D., Kutnyakov, I.V., Wilson, T.C., Burke, D.B., Williams, B.A., Bjornstad, B.N., 2001b. Geologic and geochemical data collected from vadose zone sediments from the slant borehole under SX-108 in the S/SX Waste Management Area and Preliminary Interpretations. PNNL-2001-4, Pacific Northwest National Laboratory, Richland, WA.

Smith, J.T., Comans, R.N.J., 1996. Modeling the diffusive transport and remobilization of ^{137}Cs in sediments: the effects of sorption kinetics and reversibility. Geochimica et Cosmochimica Acta 60, 995–1004.

Sobolev, V.I., 1996. Effects of potassium and nitrogen groundwater pollution on the migration of cesium-137 through the geological environment. Geokhimiya 4, 370–377.

Steefel, C.I., 2001. GIMRT, version 1.2: software for modeling multicomponent, multidimensional reactive transport. User's Guide, UCRL-MA-143182. Lawrence Livermore National Laboratory, Livermore, CA.

Steefel, C.I., in preparation. CRUNCH, software for multicomponent reactive transport: User's Guide.

Steefel, C.I., MacQuarrie, K.T.B., 1996. Approaches to modeling reactive transport in porous media. In: Lichtner, P.C., Steefel, C.I., Oelkers, E.H. (Eds.), Reactive Transport in Porous Media. Reviews in Mineralogy, vol. 34, pp. 83–125.

Steefel, C.I., Yabusaki, S.B., 1966. OS3D/GIMRT, software for multicomponent–multidimensional reactive

transport: user's manual and programmer's guide. PNL-11166, Pacific Northwest National Laboratory, Richland, WA.

Steefel, C.I., Yabusaki, S.B., 2001. Evaluation of the field exchange capacity of Hanford sediments with implications for ^{137}Cs migration. PNNL-2001-7, Pacific Northwest National Laboratory, Richland, WA.

Szerbin, P., Koblinger-Bokori, E., Koblinger, L., Vegvari, I., Ugron, A., 1999. Caesium-137 migration in Hungarian soils. Science of the Total Environment 227, 215–227.

Thirlwell, K.J., Tomlinson, W.R., Nicolls, P.E., 1995. The migration of Cs-137, Co-60 and Na-22 through a sandy aquifer-concentration profiles in laboratory columns. Radiochimica Acta 69, 113–120.

Turner, G.D., Zachara, J.M., McKinley, J.P., Smith, S.C., 1996. Surface-charge properties and UO_2^{2+} adsorption of a subsurface smectite. Geochimica et Cosmochimica Acta 60, 3399–3414.

Valocchi, A.J., Street, R.L., Roberts, P.V., 1981a. Transport of ion-exchanging solutes in groundwater: chromatographic theory and field simulation. Water Resources Research 17, 1517–1527.

Valocchi, A.J., Roberts, P.V., Parks, G.A., Street, R.L., 1981b. Simulation of the transport of ion-exchanging solutes using laboratory-determined chemical parameter values. Ground Water 19, 600–607.

Voegelin, A., Vulava, V.M., Kuhnen, F., Kretschmar, R., 2000. Multicomponent transport of major cations predicted from binary adsorption experiments. Journal of Contaminant Hydrology 46, 319–338.

Voudrias, E.A., Means, J.L., Kittel, J., 1993. Retardation of tritium and cesium in brine-saturated mudstone, halite, and carbonate porous-media. Ground Water 31, 605–615.

Ward, A.L., Gee, G.W., White, M.D., 1997. A comprehensive analysis of contaminant transport in the vadose zone beneath tank SX-109. Pacific Northwest National Laboratory Report PNNL-11463, Richland, WA.

Zachara, J.M., Smith, S.C., Liu, C., McKinley, J.P., Serne, R.J., Gassman, P.L., 2002. Sorption of Cs^+ to micaceous subsurface sediments from the Hanford site, USA. Geochimica et Cosmochimica Acta 66, 193–211.